doi:10.1093/brain/awx052 BRAIN 2017: 140; 1220–1230 | 1220

BRAIN
A JOURNAL OF NEUROLOGY

REPORT

Combined effects of scanning ultrasound and a tau-specific single chain antibody in a tau transgenic mouse model

Rebecca M. Nisbet, Ann Van der Jeugd,* Gerhard Leinenga, Harrison T. Evans, Phillip W. Janowicz and Jürgen Götz

Alzheimer's disease is characterized by the deposition of amyloid-β as extracellular plaques and hyperphosphorylated tau as intracellular neurofibrillary tangles. Tau pathology characterizes not only Alzheimer's disease, but also many other tauopathies, presenting tau as an attractive therapeutic target. Passive tau immunotherapy has been previously explored; however, because only a small fraction of peripherally delivered antibodies crosses the blood–brain barrier, enters the brain and engages with tau that forms intracellular aggregates, more efficient ways of antibody delivery and neuronal uptake are warranted. In the brain, tau exists as multiple isoforms. Here, we investigated the efficacy of a novel 2N tau isoform-specific single chain antibody fragment, RN2N, delivered by passive immunization in the P301L human tau transgenic pR5 mouse model. We demonstrate that, in treated mice, RN2N reduces anxiety-like behaviour and phosphorylation of tau at distinct sites. When administration of RN2N was combined with focused ultrasound in a scanning mode (scanning ultrasound), RN2N delivery into the brain and uptake by neurons were markedly increased, and efficacy was significantly enhanced. Our study provides evidence that scanning ultrasound is a viable tool to enhance the delivery of biologics across the blood–brain barrier and improve therapeutic outcomes and further presents single-chain antibodies as an alternative to full-length antibodies.

Clem Jones Centre for Ageing Dementia Research, Queensland Brain Institute, The University of Queensland, St Lucia Campus, Brisbane, QLD 4072, Australia

*Present address: Laboratory of Biological Psychology, Brain and Cognition, University of Leuven, 3000 Leuven, Belgium

Correspondence to: Jürgen Götz
E-mail: j.goetz@uq.edu.au

Correspondence may also be addressed to: Rebecca M. Nisbet. E-mail: r.nisbet@uq.edu.au

Keywords: blood–brain barrier; Alzheimer's disease; dementia; neurofibrillary tangles; tau

Abbreviations: scFv = single chain variable fragment; SUS = scanning ultrasound

Introduction

Alzheimer's disease is characterized by the deposition of amyloid-β as amyloid plaques and hyperphosphorylated tau as neurofibrillary tangles, together with synaptic and neuronal degeneration (Ising *et al.*, 2015; Nisbet *et al.*, 2015). Reducing tau levels abrogates amyloid-β-mediated toxicity (Ittner *et al.*, 2010), making tau an attractive therapeutic target in Alzheimer's disease. Furthermore, immunization with anti-tau antibodies has proven efficacious in multiple preclinical models (Boutajangout *et al.*, 2011; Yanamandra *et al.*, 2013; Castillo-Carranza *et al.*, 2014; Ittner *et al.*, 2015). It has been estimated, however, that only ~0.1% of a peripherally administered anti-

Received May 3, 2016. Revised January 21, 2017. Accepted January 26, 2017. Advance Access publication April 4, 2017

amyloid-β antibody enters the brain (Levites *et al.*, 2006; Golde, 2014), challenging the therapeutic potential of antibody-based treatments of neurodegenerative diseases.

We have previously shown that transiently opening the blood–brain barrier by repeated focused ultrasound in a scanning mode (scanning ultrasound, SUS) reduces the amyloid-β burden in an Alzheimer's disease mouse model (Leinenga and Götz, 2015). Others have used magnetic resonance-guided focused ultrasound to reduce amyloid-β pathology by delivering a low dose of an anti-amyloid-β antibody across the blood–brain barrier (Jordao *et al.*, 2010). However, anti-tau therapeutics present an additional challenge because they must also cross the neuronal cell membrane to interact with tau.

Single chain variable fragments (scFvs) of immunoglobulins (IgG) lack the Fc domain and are generated from fused variable domains. Their low molecular weight enables increased tissue penetration, which may facilitate transfer across the blood–brain barrier and into brain cells. An additional advantage is the lack of the Fc domain, preventing effector function-mediated inflammatory responses in the brain and microhaemorrhages (Wilcock *et al.*, 2006). Therapeutic effects have been previously demonstrated for scFvs targeting amyloid-β (Cattepoel *et al.*, 2011; Fernandez-Funez *et al.*, 2015).

Here, we have generated an anti-tau scFv, RN2N, specific for the 2N isoform of tau. We show that intravenous treatment of human 2N tau-over-expressing transgenic pR5 mice with RN2N reduces anxiety-like behaviour and tau hyperphosphorylation. Furthermore, when delivery is combined with SUS, RN2N uptake by the brain and into neurons is significantly increased, allowing for an enhanced therapeutic effect.

Materials and methods

Antibodies

Primary antibodies used for western blot (WB), immunohistochemistry (IHC) and immunofluorescence (IF) in this study were as follows: Tau 5 (Millipore; WB 1:1000), HT7 (Thermo Fisher; IHC: 1:500), AT180 and AT8 (Thermo Fisher; WB: 1:1000, IHC: 1:500), pS404 (Thermo Fisher; WB: 1:1000, IHC: 1:250), 12E8 (Prothena; WB: 1:5000; IHC: 1:2000), myc (Sigma; WB: 1:2000), EEA1 (Millipore; IF: 1:500), LAMP1 (Sigma; IF:100), p-GSK-3 β (S9; 5B3; Cell Signaling Technology; WB: 1:2000), GAPDH (Millipore; WB: 1:2000), GSK-3β (Cell Signaling Technology; WB: 1:2000). The secondary antibodies used in this study were as follows: polyclonal rabbit anti-mouse IgG biotinylated and polyclonal goat anti-rabbit IgG biotinylated (Dako; IHC: 1:500), goat anti-mouse IR680 and goat anti-rabbit IR800 (Li-cor; WB:1:10 000), and Alexa Fluor® 488 donkey anti-rabbit (Life Technologies; IF: 1:500).

Generation of the RN2N single chain variable fragment

RN2N is an scFv derived from a 2N tau-specific mouse IgG2a antibody raised against the tau peptide TEIPEGITAEEAGI (aa 84–97 of the longest human tau isoform, tau441) (Liu and Götz, 2013; Liu *et al.*, 2016*a*). The variable light (V_L) and heavy (V_H) domains were cloned as described (Johnson and Bird, 1991), joined by a (Gly4Ser)3 linker and placed in frame with an N-terminal PelB sequence and C-terminal His6 and myc tags that were synthesized (GeneArt) and cloned into the pDEST42 expression vector (Life Technologies). For determination of the IgG EC_{50}, the scFv gene was cloned into a mouse IgG2a framework (a generous gift from Stephen Mahler, The University of Queensland) as previously described (Jones *et al.*, 2010).

Expression and purification of RN2N

Expression and purification of RN2N (29.8 kDa) and a control scFv (28.2 kDa) was performed as described (Nisbet *et al.*, 2013). Endotoxins were removed using High Capacity Endotoxin Removal Resin (Pierce) and levels determined using a LAL chromogenic Endotoxin Quantification kit (Pierce).

Expression and purification of recombinant tau

Human and mouse tau expression and purification were performed as described (Liu *et al.*, 2016*a*).

ELISA

The binding specificity of purified RN2N scFv was determined using an enzyme-linked immunosorbent assay (ELISA) (Liu *et al.*, 2016*a*).

Mice

All animal experiments were conducted with female mice under the guidelines of the Australian Code of Practice for the Care and Use of Animals for Scientific Purposes and approved by the University of Queensland Animal Ethics Committee (QBI/412/14/NHMRC; QBI/027/12/NHMRC). pR5 mice express 2N4R tau with the P301L mutation under the control of the mThy.1.2 promoter (Götz *et al.*, 2001).

Generation of microbubbles

Lipid-shelled microbubbles were generated in-house (Leinenga and Götz, 2015). DSPC and DSPE-PEG2000 (Avanti Polar Lipids) were dissolved at a 9:1 molar ratio in chloroform (Sigma) and the solvent was evaporated under vacuum. The dried phospholipid cake was then dissolved in phosphate-buffered saline (PBS) with 10% glycerol to a concentration of 1 mg/ml and heated to 55°C and sonicated in a sonicator water bath. The solution was placed in 1.5 ml glass HPLC vials and the air in the vials was replaced with octafluoropropane (Arcadophta). Microbubbles were generated on the day of the experiment by agitating in a dental amalgamator at 4000 rpm for 40 s.

Scanning ultrasound device and settings

The device used was the Therapy Imaging Probe System (TIPS, Philips Research), which has an eight-element annular array

transducer with a focal length of 80 mm, a radius of curvature of 80 mm, a spherical shell of 80 mm with a 33 mm central opening, and a motorized 3D positioning system. The Focus 6 dB size (elevation × lateral × axial) was 1.5 mm × 1.5 mm × 12 mm at 1 MHz. The ultrasound settings that were applied were 1 MHz centre frequency, 0.7 MPa peak rarefactional pressure applied outside the skull, 10 Hz pulse repetition frequency, 10 ms pulse length and a 10% duty cycle. The entire forebrain of the mouse was sonicated by sequential 6 s sonications per spot.

Immunization and scanning ultrasound treatment

Four and a half-month-old pR5 mice were randomly assigned to the following groups: anaesthetic only, SUS only, RN2N only, and combined SUS and RN2N. Six to eight mice were used per experimental group and mice were treated once a week for 4 weeks. All animals were anaesthetized and prepared as previously described (Leinenga and Götz, 2015). RN2N (30 µg) and microbubble solution (30 µl) were mixed in a 29 G insulin syringe (Trumo), incubated for 2 min and then injected retro-orbitally. Animals that did not receive SUS were placed under the ultrasound transducer without ultrasound application. Animals that did receive SUS were placed in a head frame (Narishige) and SUS was applied to the entire brain as previously described (Leinenga and Götz, 2015). Upon completion of the study, anaesthetized mice were transcardially perfused with PBS, their brains harvested and the hemispheres separated. One hemisphere was snap-frozen, and the other immersion-fixed in 4% paraformaldehyde (Sigma).

Elevated plus maze

Anxiety-like behaviour was assessed by the elevated plus maze as previously described (Koss *et al.*, 2016) with some changes. Briefly, mice were placed in the central area of the maze (elevated cross-shaped apparatus with a central square, and closed as well as open arms with unprotected edges). The time spent in the three zones over a 5-min period was recorded using an overhead camera with EthovisionXT™ tracking software (Ethovision). The percentage time spent in each arm was calculated. Seven untreated wild-type littermates were used as controls. Analysis was conducted blinded.

Histology

Paraffin-embedded brain sections between Bregma −1.34 µm and −2.06 µm were analysed by immunohistochemistry as described (Ittner *et al.*, 2008), using at least four sections per mouse. The mean percentage area showing tau-positive immunoreactivity was calculated by drawing a rectangular region of interest around the amygdala and the ICH profiler plug-in for ImageJ (Varghese *et al.*, 2014). Due to the high level of background staining observed in some 12E8 sections, the use of IHC profiler plugin was not appropriate. For these sections, we defined tau-positive immunoreactivity as areas having a DAB intensity more than one standard deviation higher than the mean DAB intensity of the entire section. On sections where background staining was low, 12E8 sections were analysed by both this method and the IHC profiler which gave comparable results. Analysis was conducted blinded.

In vitro phosphorylation assay

The ability of GSK-3β to phosphorylate tau in the presence of RN2N scFv was analysed by incubating 10 µM tau alone or with either RN2N or control N1 scFv at a concentration of 0.1, 1 and 10 µM, respectively, for 1 h at room temperature. Samples were then incubated with or without 9 units GSK-3β and 80 µM ATP in kinase buffer (New England Biosciences) at 30°C for 8 h. Phosphorylation was determined by electrophoresis on 10% polyacrylamide gels followed by Coomassie staining or western blotting with the phosphorylated tau-specific antibodies AT8, AT180, 12E8, pSer404, as well as Tau5 for total tau and myc for myc-tagged scFv detection using the LiCor Odyssey system.

RN2N brain delivery assessment

RN2N was conjugated with Alexa Fluor® 647 (Thermo Fisher) and purified by size exclusion chromatography using a Superdex 200 10/300 column (GE Healthcare) equilibrated in PBS pH 7.4 at 0.5 ml/min.

pR5 mice aged 6 or 8 months were randomly assigned to the following groups: SUS only, RN2N only and combined SUS and RN2N. Three mice were used per group and treatment was conducted as described above. Different from above, to assess antibody delivery pR5 mice were injected with a higher dose of 90 µg RN2N. At 30 min after delivery, mice were given an overdose of sodium pentabarbitone and transcardially perfused with PBS. The brains were dissected as described above. For analysis of brain uptake of Alexa Fluor® 647-conjugated RN2N, the fixed hemispheres of the mice were imaged in a LI-COR Odyssey Fc near-infrared scanner (700 nm laser 2 min scan time) before being cryo-protected by immersion in 30% sucrose and then sectioned at 40-µm thickness on a freezing sliding microtome. For immunofluorescence, sections were incubated with primary antibodies against tau (HT7), EEA1 and LAMP1 overnight, followed by 2 h incubation in Alexa Fluor® 488-conjugated secondary antibodies. Sections were mounted on slides and stained with 1 µg/ml DAPI in PBS for 10 min, and cover-slipped with fluorescent mounting medium (Dako). Images were taken with a Zeiss LSM510 scanning confocal microscope.

Statistical analysis

Statistical analysis was performed with GraphPad Prism 6.0c software using one-way ANOVA or *t*-test. All values are given as mean ± standard error of the mean (SEM).

Results

RN2N single chain variable fragment is specific for the 2N tau isoform

In the human brain, six major tau isoforms are generated through alternative splicing. They differ by the presence of zero, one or two amino-terminal inserts (0N, 1N or 2N),

and the presence of three or four microtubule-binding repeat domains. We have previously performed co-immunoprecipitations followed by mass spectrometry, which suggested that 2N tau interacts preferentially with proteins implicated in neurodegenerative diseases (Liu *et al.*, 2016*a*). We therefore raised a monoclonal antibody, RN2N IgG, specific for human and mouse 2N tau (Supplementary Fig. 1A). The specificity of RN2N IgG was confirmed by western blotting (Supplementary Fig. 1B) and compared to the monoclonal antibody, Tau-5, that recognizes all tau isoforms (Supplementary Fig. 1B). To minimize the size and remove the potentially immunogenic Fc region, we generated an RN2N scFv by genetically fusing the V_H and V_L chains. The resulting myc-tagged antibody fragment existed as a stable monomer (Supplementary Fig. 1C) and had an approximate size of 28 kDa (Supplementary Fig. 1D).

To ensure uncompromised binding and specificity of RN2N scFv to 2N tau, ELISA was performed. While the binding of RN2N scFv to tau was reduced compared to the parental IgG (EC_{50} of 86 nM for the scFv compared to 12 nM for the IgG) (Supplementary Fig. 1E), its specificity for 2N tau was, however, retained (Supplementary Fig. 1F).

RN2N single chain variable fragment combined with scanning ultrasound reduces anxiety in pR5 tau transgenic mice

We next sought to determine whether passive immunization with RN2N ameliorates the tau-related phenotype *in vivo* and to investigate the effect of combining delivery with SUS (Fig. 1A). The pR5 strain presents with a progressive tau pathology in several brain areas that is initiated with pronounced accumulation of hyperphosphorylated tau in the amygdala from around 4 months of age onwards (Götz *et al.*, 2001; Pennanen *et al.*, 2004). The amygdala is involved in creating, maintaining and modifying anxiety and fear responses. Furthermore, increased anxiety is commonly observed in patients with Alzheimer's disease or frontotemporal lobar degeneration (FTLD) (Porter *et al.*, 2003), and increased anxiety-like behaviour has been found in FTLD-Tau mouse models, as assessed by the elevated plus maze (Walf and Frye, 2007; Koss *et al.*, 2016). Age-matched pR5 mice were split into four treatment groups (Fig. 1B). The first underwent anaesthesia only, the second received microbubbles followed by SUS, the third received RN2N, and the fourth received both microbubbles and RN2N followed by SUS (Fig. 1B). SUS was conducted under settings that have previously been shown to cause no damage (Leinenga and Götz, 2015). A group of wild-type mice did not undergo any treatment. pR5 mice were treated once per week for 4 consecutive weeks, after which anxiety-like behaviour was tested in the elevated plus maze (Fig. 1C). To ensure the anaesthetic was not having an effect on anxiety, wild-type mice were treated for 4 weeks with anaesthetic and compared to untreated mice. No significant difference in the percentage time spent in the open arm was observed between these groups (16.44 ± 3.74 of total time for the treated group compared to 13 ± 3.70 for the untreated group, $n = 6$, mean $\pm$ SEM). pR5 mice demonstrated increased anxiety-like behaviour characterized by a decreased percentage time spent in the open arms (2% of total time for pR5 mice compared to 18% for wild-type controls) (Fig. 1D and E). Treatment with RN2N alone resulted in a slight but significant increase in the percentage time spent in the open arms (6%) that was not observed in the SUS only group (2%) (Fig. 1D and E). Combining RN2N and SUS, however, further increased the percentage time spent in the open arms (10%) (Fig. 1D and E), suggesting that RN2N is capable of reducing anxiety-like behaviour in pR5 mice, an effect that is greatly improved when RN2N is delivered with SUS.

RN2N delivery in combination with scanning ultrasound reduces phosphorylated tau levels in pR5 mice

We next determined if the behavioural improvement observed with RN2N alone or in combination with SUS was associated with a reduction in tau hyperphosphorylation.

While western blotting and ELISA of total brain homogenate were not sensitive enough to accurately detect p-tau levels in the treated mice, staining of brain sections for tau phosphorylated at the AT8 epitope pSer202/pThr205 (Biernat *et al.*, 1992) and the AT180 epitope pThr231 (Goedert *et al.*, 1994; Amniai *et al.*, 2011), both major phosphorylation sites in tauopathy and pR5 mice revealed phosphorylated tau predominantly in the amygdala (Fig. 2A–D) (Deters *et al.*, 2008). The total AT8-immunoreactive area in the amygdala of the pR5 group was 51% (Fig. 2C). Treatment with RN2N or SUS alone significantly reduced the AT8-immunoreactive area to 33% and 34%, respectively, compared to the pR5 control (Fig. 2D). Treatment with the combination of RN2N and SUS further reduced the AT8-immunoreactive area to 15% (Fig. 2C). These results were mirrored by those observed with AT180, with the total AT180-immunoreactive area in the amygdala of the pR5 group being 57% (Fig. 2D). Treatment with RN2N or SUS alone significantly reduced the AT180-immunoreactive area to 37% and 36%, respectively, compared to the pR5 control (Fig. 2D). Combined treatment with RN2N and SUS further reduced the immunoreactive area to 17% (Fig. 2D). In contrast, the total 12E8-immunoreactive area in the amygdala of the pR5 group was 36% and treatment with RN2N or SUS alone did not reduce this (Fig. 2E). The combined treatment however, reduced the 12E8-immunoreactive area to 20% compared to the pR5 only (Fig. 2E). Furthermore, the total pSer404-immunoreactive area in the amygdala of the pR5 mice was

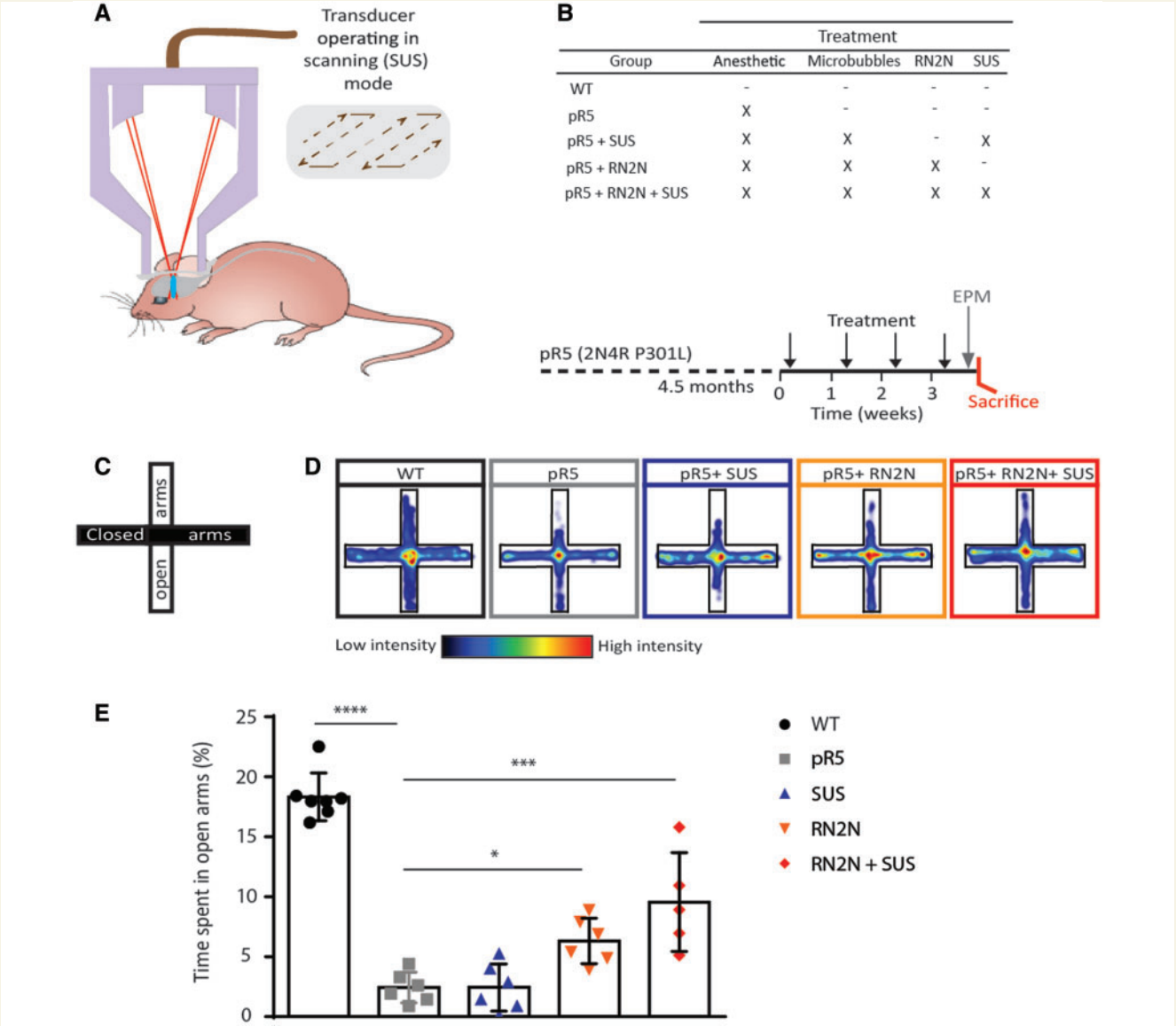

Figure 1 RN2N treatment in combination with SUS reduces anxiety-like behaviour in pR5 tau transgenic mice. (**A**) Schematic of ultrasound treatment using a transducer in scanning (SUS) mode in order to achieve microbubble-assisted opening of the blood–brain barrier. (**B**) Female pR5 mice at 4.5 months of age were randomly assigned to one of four groups: pR5, pR5 + SUS, pR5 + RN2N and pR5 + RN2N + SUS and treated as indicated (X) once a week for 4 weeks. A group of wild-type (WT) littermate controls did not undergo any treatment. Upon treatment completion, mice were analysed on the elevated plus maze (EPM), and then sacrificed. (**C**) The elevated plus maze is an elevated cross-shaped apparatus with a central square and 15 cm long × 5 cm wide closed arms with a 15 cm wall and open arms with unprotected edges. (**D**) The mean positional heat map within the elevated plus maze for each treatment group. (**E**) pR5 mice ($n = 6$) spend significantly less time in the open arms compared to wild-type mice ($n = 7$) (****$P < 0.0001$). No difference was observed in the pR5 + SUS group ($n = 6$) compared to the pR5 mice. However, mice in the pR5 + RN2N group ($n = 6$) and those in the pR5 + RN2N + SUS group ($n = 5$) spent significantly more time in the open arms than pR5 mice (*$P = 0.03$ and ***$P = 0.0002$, respectively), indicating a reduction in anxiety-like behaviour (mean ± SEM; one-way ANOVA with Dunnett's multiple comparison test).

35% and this was not reduced in any of the treatment groups (Fig. 2F). Preliminary work demonstrated a significant reduction (17%, $P = 0.008$, *t*-test) of total GSK3, but not p-GSK3, in the brains of the SUS-only treated group compared to the anaesthetic only controls, which may explain the decreased p-tau levels in this treatment group.

RN2N inhibits GSK3-mediated tau phosphorylation *in vitro*

Glycogen synthase kinase 3β (GSK3β) is a serine/threonine kinase that is known to phosphorylate tau on most serine and threonine residues (Hernandez *et al.*, 2013). Furthermore, increased GSK3β activity has previously

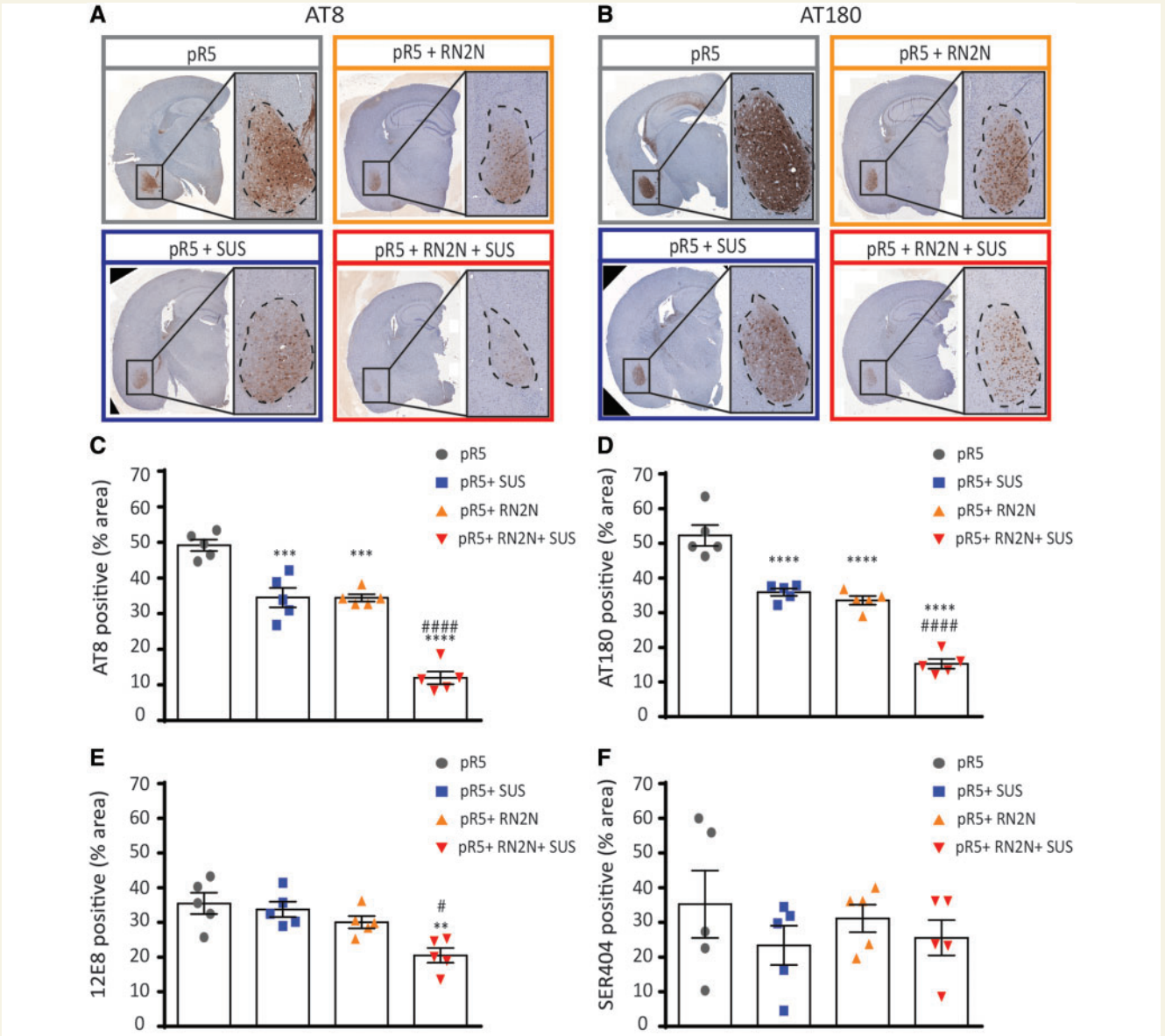

Figure 2 Delivery of RN2N in combination with SUS significantly reduces phosphorylated tau levels in the amygdala. (**A**) Representative images of the AT8 phosphorylated tau immunoreactivity observed in a full brain section and amygdala of pR5 mice in each treatment group (Scale bar = 100 μm). (**B**) Representative images of the AT180 phosphorylated tau immunoreactivity observed in the amygdala of pR5 mice in each treatment group (Scale bar = 100 μm). (**C**) AT8 phosphorylated tau in the amygdala was significantly reduced in all treatment groups compared to the pR5 group (****$P \leqslant 0.0001$). Comparison of the pR5 + RN2N + SUS group to the pR5 + SUS and pR5 + RN2N groups demonstrates a further reduction in AT8 tau-positive area in the amygdala (#####$P \leqslant 0.0001$). (**D**) AT180 phosphorylated tau in the amygdala was significantly reduced in all treatment groups compared to the pR5 group (****$P \leqslant 0.0001$). Comparison of the pR5 + RN2N + SUS group to the pR5 + SUS and pR5 + RN2N groups demonstrates a further reduction in AT180 tau-positive area in the amygdala (####$P = 0.0002$). (**E**) 12E8 phosphorylated tau in the amygdala was significantly reduced in the RN2N + SUS group compared to the pR5 group (**$P < 0.01$), and was reduced in comparison to pR5 + SUS and pR5 + RN2N groups (#$P \leqslant 0.05$). (**F**) Ser404 phosphorylated tau in the amygdala was not significantly reduced in any treatment group compared to the pR5 group (mean ± SEM, one-way ANOVA with Tukey's multiple comparison test, $n = 5$).

been reported to be responsible for tau hyperphosphorylation and converting amorphous into fibrillar tau in pR5 mice (Köhler *et al.*, 2013). To determine whether RN2N binding to tau inhibits GSK3β, recombinant human tau was incubated in the presence of RN2N and GSK3β. Although tau did undergo phosphorylation in the presence of RN2N scFv, as indicated by the mobility shift of tau, AT8 and AT180 phosphorylation were inhibited (Fig. 3A and B). This was not observed when tau was incubated in the presence of the control scFv, suggesting that inhibition of AT8 and AT180 phosphorylation occurs because of a direct interaction between tau and RN2N scFv (Fig. 3A). In

contrast, phosphorylation at the C-terminal epitopes, 12E8 and Ser404, was not inhibited in the presence of RN2N (Fig. 3A), suggesting that RN2N inhibition of GSK3β phosphorylation is limited to the N-terminus of tau.

Ultrasound-enhanced RN2N delivery across the blood–brain barrier leads to neuronal uptake

To investigate whether the enhanced therapeutic effect of RN2N when delivered by SUS was due to increased levels of brain RN2N, we delivered Alexa Fluor® 647-conjugated RN2N with microbubbles into the peripheral circulation and performed SUS or sham treatment. Using Li-COR infrared imaging, Alexa Fluor® 647-labelled RN2N was detectable in the brain of both 6- and 8-month-old pR5 mice 30 min after SUS treatment, but not when RN2N was injected without SUS, or when SUS was applied without RN2N (Fig. 4A). When quantified, the mean scFv fluorescent intensity in the brain increased from 57.7 to 662 arbitrary units when SUS was applied (11-fold increase) (Fig. 4A). Furthermore, confocal imaging of brain sections showed widespread hippocampal and cortical delivery of RN2N when SUS was applied (Fig. 4B). The cytoarchitecture of the hippocampus allowed demonstrating not only an uptake and distribution into the cell body, but also into proximal and distal dendrites, a compartment where tau toxicity is believed to be exerted (Fig. 4B, inset). To determine if RN2N is contained within endosomes or lysosomes, we performed immunofluorescence for EEA1 (Fig. 4C) and LAMP1 (Fig. 4D). These stainings indicate that RN2N is not confined to the endosomal pathway after uptake and is distributed throughout neurons. Importantly, neuronal uptake of RN2N was also observed in the amygdala after SUS treatment where it co-localized with tau (Fig. 4E). We therefore conclude that the enhanced effect of RN2N when delivered by SUS occurs conjointly with increased brain levels and efficient neuronal uptake of the scFv.

Discussion

Here we show that a tau-isoform specific scFv, RN2N, can reduce anxiety-like behaviour and tau phosphorylation in pR5 mice, and that this effect is significantly enhanced when delivery is combined with SUS. RN2N specifically recognizes the 2N tau isoform, which has not previously been targeted therapeutically. In the adult human brain, 2N tau is under-represented compared to the 0N and 1N isoforms and is estimated to comprise ~9% of total tau (Goedert and Jakes, 1990). Considering that 2N tau has been implicated in neurodegenerative diseases (Liu *et al.*, 2016*a*), targeting only this subset of tau may be sufficient to delay or halt the disease.

We have demonstrated *in vitro* that RN2N inhibits the GSK3β phosphorylation of tau at N-terminal sites (Ser202 and Thr231) but not at a C-terminal site (Ser404). GSK3β is a proline-directed kinase that plays a major role in regulating tau under both physiological and pathological conditions (Cho and Johnson, 2003; Hanger and Noble, 2011). GSK3β can phosphorylate its substrate on either unprimed Ser/Thr-Pro motifs or a primed motif {(S/T)XXX(S/T)[P]}, which is first phosphorylated at a serine or threonine, four residues C-terminal to its target (Cho and Johnson, 2003). We therefore hypothesize that binding of RN2N to tau prevents the interaction between GSK3β and tau required for phosphorylation of more N-terminal epitopes. This may be caused by direct blocking of GSK3β or alternatively, as some GSK3β phosphorylated epitopes require a prior phosphorylation by a priming kinase, it is possible that RN2N blocks the priming required for GSK3β phosphorylation at the more N-terminal epitopes. Our *in vitro* data could explain the reduction in tau phosphorylation that we observed at the AT8, AT180 and to a lesser extent 12E8 epitopes after treatment with RN2N and SUS in the pR5 mice, although further work is required to determine the exact mechanism. Nonetheless, it is reasonable to assume that the reduction in phosphorylated tau in the amygdala after the combined RN2N and SUS treatment led to a reduction in anxiety-like behaviour characteristic of the pR5 mice. Future studies will determine whether this treatment strategy can also clear phosphorylated tau and prevent memory impairment in older pR5 mice.

We had aimed to determine changes in tau levels and tau phosphorylation by both ELISA and western blotting; however, because the mice were analysed at an age of disease onset with low total levels of p-tau, levels of different forms of p-tau were at or below the limit of detection. Therefore, we used immunohistochemistry, which allowed us to monitor changes in p-tau in the amygdala, where disease in the pR5 mice is initiated. Interestingly, we also observed reduced tau phosphorylation in the SUS-only group, suggesting that SUS may specifically influence tau phosphorylation. However, as no decrease in anxiety-like behaviour was observed in this group, the mechanism by which SUS decreases tau phosphorylation most likely differs from that of RN2N. Ultrasound has previously been demonstrated to increase the ubiquitination of proteins specifically within neurons (Alonso *et al.*, 2010). It is therefore possible that SUS increases the turnover of phosphorylated tau in the pR5 mice through the ubiquitin pathway. One possible mechanism by which SUS is reducing tau phosphorylation is by an effect on kinases such as GSK3. Preliminary work from our group demonstrated a significant reduction of total GSK3, but not p-GSK3, in the brains of the SUS-only treated group compared to the anaesthetic only controls, which may also explain the decrease in p-tau levels in this treatment group. We have not analysed other kinases at this stage, and plan to explore this further. Investigating the role of SUS alone in tau transgenic mice as well as the underlying mechanisms will determine if this approach can be used as a therapy for Alzheimer's disease and related tauopathies.

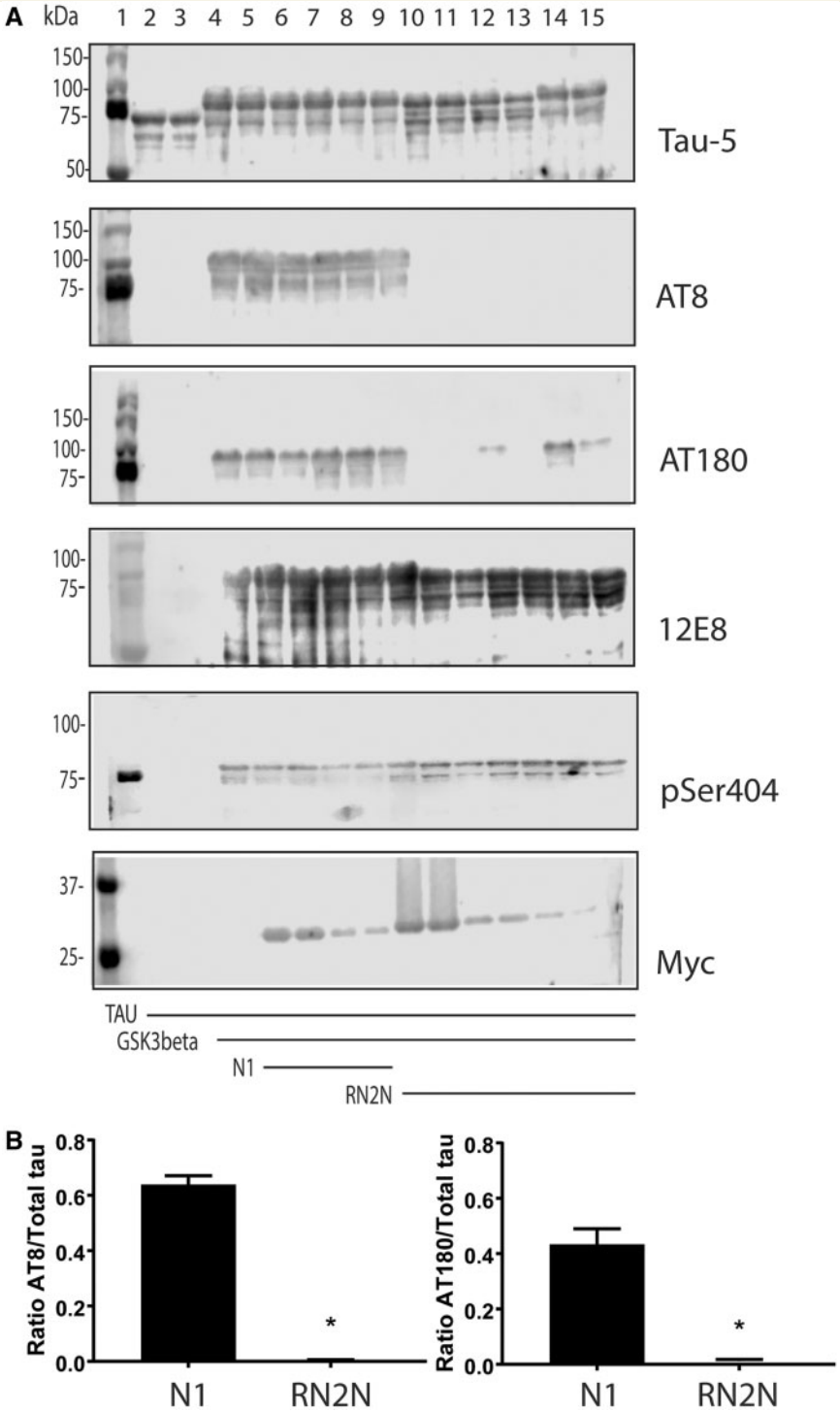

Figure 3 RN2N inhibits GSK3β phosphorylation of tau *in vitro*. (**A**) GSK3β phosphorylates tau at multiple serine and threonine epitopes resulting in a molecular weight shift of tau. Lane 1: molecular weight marker; lanes 2 and 3: tau alone; lanes 4 and 5: tau incubated with GSK3β; lanes 6 and 7: tau incubated with GSK3β in the presence of 10 μM N1 control scFv; lanes 8 and 9: tau incubated with GSK3β in the presence of 1 μM N1 control scFv; lanes 10 and 11: tau incubated with GSK3β in the presence of 10 μM RN2N; lanes 12 and 13: tau incubated with GSK3β in the presence of 1 μM RN2N; and lanes 14 and 15: tau incubated with GSK3β in the presence of 0.1 μM RN2N. Co-treatment of tau and GSK3β with RN2N leads to reduced phosphorylation at the AT8 and AT180 epitopes, quantified in **B**, with no change to 12E8 or pSer404 epitopes. Blotting for myc indicates the presence of scFv. (**B**) Quantification of the reduction of phosphorylation of the AT8 and AT180 epitopes with 10 μM RN2N compared to 10 μM N1 control scFv ($P < 0.05$) (mean ± SEM, *t*-test).

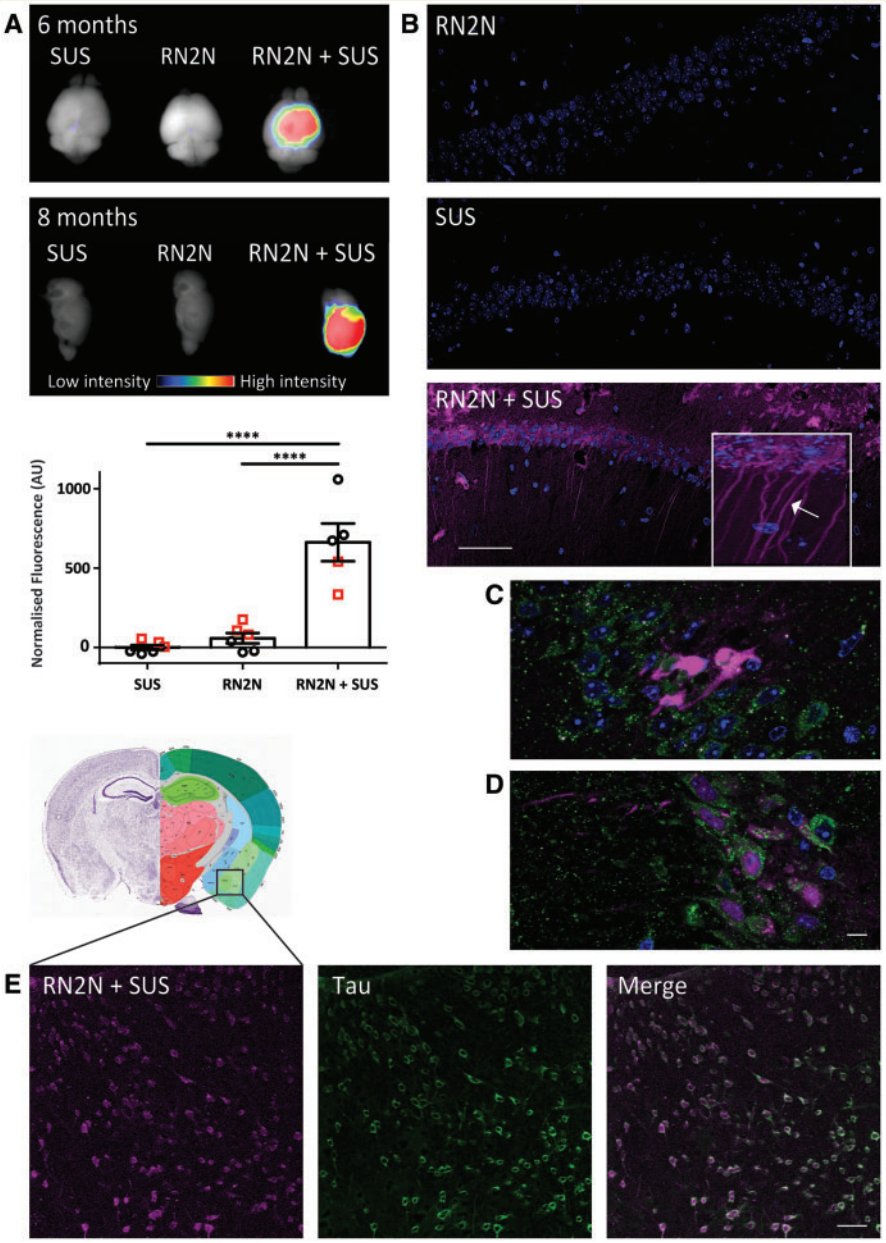

Figure 4 SUS enhances RN2N scFv delivery across the blood–brain barrier and into neurons. pR5 mice under anaesthesia were injected retro-orbitally with either microbubbles only (SUS), RN2N conjugated to Alexa 647 only (RN2N) or a combination of both (RN2N + SUS). SUS was then applied to SUS and RN2N + SUS groups. After 30 min mice were sacrificed and tissue analysed by fluorescence imaging. (**A**) Fluorescence imaging indicates widespread brain uptake of RN2N in 6-month and 8-month-old RN2N + SUS treated mice. Quantification of the fluorescent intensity demonstrates an approximate 11-fold increase in scFv uptake in the RN2N + SUS treated mice (mean = 662 ± 119) compared to the RN2N only treated mice (mean = 58 ± 32) (grouping 6-month-old mice = red squares; and 8-month-old mice = black circles; mean ± SEM, $P < 0.0001$, one-way ANOVA with Tukey's post-test). (**B**) Post-sectioning, RN2N was only detectable in the RN2N + SUS treated mice as shown for the CA1 region of the hippocampus. *Inset:* Zoomed-in image of RN2N + SUS treated mouse brain tissue with RN2N observed within neuronal cell bodies and apical dendrites (arrow). (**C**) Co-immunofluorescence staining for EEA1 (green) and RN2N (magenta) and (**D**) LAMP1 (green) and RN2N (magenta) indicates that the internalized RN2N is not confined to endosomes or lysosomes (Scale bar = 10 μm). (**E**) In the RN2N + SUS treated mice, RN2N is also observed in the amygdala where it co-localized with HT7 staining (human tau). Coronal image sourced from Allen Mouse Brain Atlas (2004) (Scale bar = 50 μm).

In addition to demonstrating that a 2N tau isoform-specific scFv reduces anxiety-like behaviour and tau phosphorylation *in vivo*, we have also demonstrated that SUS enhances RN2N delivery across the blood–brain barrier and into neurons. Focused ultrasound has previously been demonstrated to increase the CNS uptake of a full-sized IgG by 5.7 to 56.7-fold (Liu *et al.*, 2016*b*). Although we did not compare the delivery of the RN2N IgG to that of

the scFv, it is possible that the smaller size of the scFv compared to a full-sized antibody may optimize SUS-mediated delivery of RN2N into the brain. Ultrasound delivery studies using dextrans of varying sizes suggest that this might be the case, with smaller dextrans being delivered into the brain at higher levels and more homogenously with ultrasound than larger dextrans. This also correlates with ultrasound pressure, suggesting, from a safety point of view, that there is a size limit associated with the technique (Choi *et al.*, 2010). Furthermore, *in vitro* ultrasound-enhanced cellular uptake of different dextrans demonstrated that, although the percentage of cells that internalized dextran was independent of the molecular weight, the number of internalized molecules was higher for smaller dextrans (Afadzi *et al.*, 2013). Increased neuronal uptake of an anti-tau scFv compared to the IgG has previously been shown in a tau transgenic mouse model after intracarotid injection (Krishnaswamy *et al.*, 2014). Increased neuronal delivery has also been demonstrated with an anti-tau fragment antigen-binding (Fab) fragment compared to the IgG *in vitro* (Gu *et al.*, 2013). These studies suggest that the scFv format of RN2N may also enhance its SUS-mediated neuronal uptake. The mechanism by which RN2N enters the neuron, however, is yet to be investigated. Previous studies with anti-tau antibodies have demonstrated that antibody uptake levels correlate with neuronal tau levels, suggesting that the presence of tau is required for the antibody uptake (Congdon *et al.*, 2013; Collin *et al.*, 2014). This process primarily occurs via clathrin-dependent FcγII/III endocytosis (Congdon *et al.*, 2013). Interestingly, bulk endocytosis is the major mechanism by which ultrasound-enhanced cellular internalization of dextran occurs (Afadzi *et al.*, 2013) and is the proposed mechanism by which an anti-tau Fab fragment is thought to be internalized (Gu *et al.*, 2013), presenting a similar mechanism for SUS-enhanced neuronal uptake of RN2N, despite the lack of the Fc region. Following neuronal uptake we observed RN2N was not confined to endosomes and therefore avoids immediate lysosomal degradation. It is therefore likely that RN2N binds to tau in the cytoplasm. Whilst the mechanism by which RN2N escapes endosomes in unknown, it is possible that this process is mediated by the C-terminal histidine tag. In drug delivery, histidine rich peptides are widely used as powerful endosomal escape agents. Within endosomes, the imidazole group of histidine gets protonated under the acidic conditions. This step recruits chloride ions, which results in osmotic swelling and endosomal cracking leading to the cytoplasmic release of the histidine-tagged molecule (Vazquez *et al.*, 2008; Ferrer-Miralles *et al.*, 2011).

In summary, we have demonstrated that passive immunization against 2N tau with RN2N scFv effectively decreases tau phosphorylation and anxiety-like behaviour in pR5 mice. Furthermore, SUS-enhanced delivery of RN2N significantly increases its efficacy by increasing the amount of antibody delivered to the brain, as well as into neurons, where tau is predominately localized. While RN2N only targets a subset of tau and its ability to reduce tau pathology in a model expressing all isoforms of tau needs to be investigated, our proof-of-principle study demonstrates SUS may be applied to any therapeutic antibody to increase their efficacy. The therapeutic delivery combined with SUS could offer significant clinical benefits for the treatment of patients with Alzheimer's disease and related tauopathies by reducing both treatment cost and duration.

Acknowledgements

We thank Matthew Pelekanos, Tishila Palliyaguru, Linda Cumner, David Brici, Martina Jones and Marianne Gillard for excellent technical assistance and Rowan Tweedale for critical reading of the manuscript.

Funding

This research was supported by the estate of Dr Clem Jones AO, the State Government of Queensland, the Federal Government of Australia (ACT900116), and by grants from The Brain Foundation to R.M.N. and the Australian Research Council (DP13300101932) and the National Health and Medical Research Council of Australia (APP1037746, APP1003150) to J.G. R.M.N. is a recipient of the Alzheimer's Australia Dementia Research Foundation Fellowship and Yulgilbar Alzheimer's Research Program Fellowship. A.vd J. is supported by a FWO fellowship.

Supplementary material

Supplementary material is available at *Brain* online.

References

Afadzi M, Strand SP, Nilssen EA, Masoy SE, Johansen TF, Hansen R, et al. Mechanisms of the ultrasound-mediated intracellular delivery of liposomes and dextrans. IEEE Trans Ultrason Ferroelectr Freq Control 2013; 60: 21–33.

Alonso A, Reinz E, Fatar M, Jenne J, Hennerici MG, Meairs S. Neurons but not glial cells overexpress ubiquitin in the rat brain following focused ultrasound-induced opening of the blood-brain barrier. Neuroscience 2010; 169: 116–24.

Amniai L, Lippens G, Landrieu I. Characterization of the AT180 epitope of phosphorylated Tau protein by a combined nuclear magnetic resonance and fluorescence spectroscopy approach. Biochem Biophys Res Commun 2011; 412: 743–6.

Biernat J, Mandelkow EM, Schroter C, Lichtenberg-Kraag B, Steiner B, Berling B, et al. The switch of tau protein to an Alzheimer-like state includes the phosphorylation of two serine-proline motifs upstream of the microtubule binding region. EMBO J 1992; 11: 1593–7.

Boutajangout A, Ingadottir J, Davies P, Sigurdsson EM. Passive immunization targeting pathological phospho-tau protein in a mouse model reduces functional decline and clears tau aggregates from the brain. J Neurochem 2011; 118: 658–67.

Castillo-Carranza DL, Sengupta U, Guerrero-Munoz MJ, Lasagna-Reeves CA, Gerson JE, Singh G, et al. Passive immunization with Tau oligomer monoclonal antibody reverses tauopathy phenotypes without affecting hyperphosphorylated neurofibrillary tangles. J Neurosci 2014; 34: 4260–72.

Cattepoel S, Hanenberg M, Kulic L, Nitsch RM. Chronic intranasal treatment with an anti-Abeta(30–42) scFv antibody ameliorates amyloid pathology in a transgenic mouse model of Alzheimer's disease. PLoS One 2011; 6: e18296.

Cho JH, Johnson GV. Glycogen synthase kinase 3beta phosphorylates tau at both primed and unprimed sites. Differential impact on microtubule binding. J Biol Chem 2003; 278: 187–93.

Choi JJ, Wang S, Tung YS, Morrison B III, Konofagou EE. Molecules of various pharmacologically-relevant sizes can cross the ultrasound-induced blood-brain barrier opening *in vivo*. Ultrasound Med Biol 2010; 36: 58–67.

Collin L, Bohrmann B, Gopfert U, Oroszlan-Szovik K, Ozmen L, Gruninger F. Neuronal uptake of tau/pS422 antibody and reduced progression of tau pathology in a mouse model of Alzheimer's disease. Brain 2014; 137: 2834–46.

Congdon EE, Gu J, Sait HB, Sigurdsson EM. Antibody uptake into neurons occurs primarily via clathrin-dependent Fcgamma receptor endocytosis and is a prerequisite for acute tau protein clearance. J Biol Chem 2013; 288: 35452–65.

Deters N, Ittner LM, Götz J. Divergent phosphorylation pattern of tau in P301L tau transgenic mice. Eur J Neurosci 2008; 28: 137–47.

Fernandez-Funez P, Zhang Y, Sanchez-Garcia J, de Mena L, Khare S, Golde TE, et al. Anti-A beta single-chain variable fragment antibodies exert synergistic neuroprotective activities in Drosophila models of Alzheimer's disease. Hum Mol Genet 2015; 24: 6093–105.

Ferrer-Miralles N, Corchero JL, Kumar P, Cedano JA, Gupta KC, Villaverde A, et al. Biological activities of histidine-rich peptides; merging biotechnology and nanomedicine. Microb Cell Fact 2011; 10: 101.

Goedert M, Jakes R. Expression of separate isoforms of human tau protein: correlation with the tau pattern in brain and effects on tubulin polymerization. EMBO J 1990; 9: 4225–30.

Goedert M, Jakes R, Crowther RA, Cohen P, Vanmechelen E, Vandermeeren M, et al. Epitope mapping of monoclonal antibodies to the paired helical filaments of Alzheimer's disease: identification of phosphorylation sites in tau protein. Biochem J 1994; 301 (Pt 3): 871–7.

Golde TE. Open questions for Alzheimer's disease immunotherapy. Alzheimers Res Ther 2014; 6: 3.

Götz J, Chen F, Barmettler R, Nitsch RM. Tau filament formation in transgenic mice expressing P301L tau. J Biol Chem 2001; 276: 529–34.

Gu J, Congdon EE, Sigurdsson EM. Two novel Tau antibodies targeting the 396/404 region are primarily taken up by neurons and reduce Tau protein pathology. J Biol Chem 2013; 288: 33081–95.

Hanger DP, Noble W. Functional implications of glycogen synthase kinase-3-mediated tau phosphorylation. Int J Alzheimers Dis 2011; 2011: 352805.

Hernandez F, Lucas JJ, Avila J. GSK3 and tau: two convergence points in Alzheimer's disease. J Alzheimers Dis 2013; 33 (Suppl 1): S141–4.

Ising C, Stanley M, Holtzman DM. Current thinking on the mechanistic basis of Alzheimer's and implications for drug development. Clin Pharmacol Ther 2015; 98: 469–71.

Ittner A, Bertz J, Suh LS, Stevens CH, Götz J, Ittner LM. Tau-targeting passive immunization modulates aspects of pathology in tau transgenic mice. J Neurochem 2015; 132: 135–45.

Ittner LM, Fath T, Ke YD, Bi M, van Eersel J, Li KM, et al. Parkinsonism and impaired axonal transport in a mouse model of frontotemporal dementia. Proc Natl Acad Sci USA 2008; 105: 15997–6002.

Ittner LM, Ke YD, Delerue F, Bi M, Gladbach A, van Eersel J, et al. Dendritic function of tau mediates amyloid-beta toxicity in Alzheimer's disease mouse models. Cell 2010; 142: 387–97.

Johnson S, Bird RE. Construction of single-chain Fv derivatives monoclonal antibodies and their production in Escherichia coli. Methods Enzymol 1991; 203: 88–98.

Jones ML, Seldon T, Smede M, Linville A, Chin DY, Barnard R, et al. A method for rapid, ligation-independent reformatting of recombinant monoclonal antibodies. J Immunol Methods 2010; 354: 85–90.

Jordao JF, Ayala-Grosso CA, Markham K, Huang Y, Chopra R, McLaurin J, et al. Antibodies targeted to the brain with image-guided focused ultrasound reduces amyloid-beta plaque load in the TgCRND8 mouse model of Alzheimer's disease. PLoS One 2010; 5: e10549.

Köhler C, Dinekov M, Götz J. Active glycogen synthase kinase-3 and tau pathology-related tyrosine phosphorylation in pR5 human tau transgenic mice. Neurobiol Aging 2013; 34: 1369–79.

Koss DJ, Robinson L, Drever BD, Plucinska K, Stoppelkamp S, Veselcic P, et al. Mutant Tau knock-in mice display frontotemporal dementia relevant behaviour and histopathology. Neurobiol Dis 2016; 91: 105–23.

Krishnaswamy S, Lin Y, Rajamohamedsait WJ, Rajamohamedsait HB, Krishnamurthy P, Sigurdsson EM. Antibody-derived *in vivo* imaging of tau pathology. J Neurosci 2014; 34: 16835–50.

Leinenga G, Götz J. Scanning ultrasound removes amyloid-beta and restores memory in an Alzheimer's disease mouse model. Sci Transl Med 2015; 7: 278ra33.

Levites Y, Smithson LA, Price RW, Dakin RS, Yuan B, Sierks MR, et al. Insights into the mechanisms of action of anti-Abeta antibodies in Alzheimer's disease mouse models. FASEB J 2006; 20: 2576–8.

Liu C, Götz J. Profiling murine tau with 0N, 1N and 2N isoform-specific antibodies in brain and peripheral organs reveals distinct subcellular localization, with the 1N isoform being enriched in the nucleus. PLoS One 2013; 8: e84849.

Liu C, Song X, Nisbet R, Götz J. Co-immunoprecipitation with tau isoform-specific antibodies reveals distinct protein interactions, and highlights a putative role for 2N tau in disease. J Biol Chem 2016a; 291: 8173–88.

Liu HL, Hsu PH, Lin CY, Huang CW, Chai WY, Chu PC, et al. Focused ultrasound enhances central nervous system delivery of Bevacizumab for Malignant Glioma treatment. Radiology 2016b; 281: 99–108.

Nisbet RM, Nigro J, Breheney K, Caine J, Hattarki MK, Nuttall SD. Central amyloid-beta-specific single chain variable fragment ameliorates Abeta aggregation and neurotoxicity. Protein Eng Des Sel 2013; 26: 571–80.

Nisbet RM, Polanco JC, Ittner LM, Götz J. Tau aggregation and its interplay with amyloid-beta. Acta Neuropathol 2015; 129: 207–20.

Pennanen L, Welzl H, D'Adamo P, Nitsch RM, Götz J. Accelerated extinction of conditioned taste aversion in P301L tau transgenic mice. Neurobiol Dis 2004; 15: 500–9.

Porter VR, Buxton WG, Fairbanks LA, Strickland T, O'Connor SM, Rosenberg-Thompson S, et al. Frequency and characteristics of anxiety among patients with Alzheimer's disease and related dementias. J Neuropsychiatry Clin Neurosci 2003; 15: 180–6.

Varghese F, Bukhari AB, Malhotra R, De A. IHC Profiler: an open source plugin for the quantitative evaluation and automated scoring of immunohistochemistry images of human tissue samples. PLoS One 2014; 9: e96801.

Vazquez E, Ferrer-Miralles N, Villaverde A. Peptide-assisted traffic engineering for nonviral gene therapy. Drug Discov Today 2008; 13: 1067–74.

Walf AA, Frye CA. The use of the elevated plus maze as an assay of anxiety-related behavior in rodents. Nat Protoc 2007; 2: 322–8.

Wilcock DM, Alamed J, Gottschall PE, Grimm J, Rosenthal A, Pons J, et al. Deglycosylated anti-amyloid-beta antibodies eliminate cognitive deficits and reduce parenchymal amyloid with minimal vascular consequences in aged amyloid precursor protein transgenic mice. J Neurosci 2006; 26: 5340–6.

Yanamandra K, Kfoury N, Jiang H, Mahan TE, Ma S, Maloney SE, et al. Anti-tau antibodies that block tau aggregate seeding *in vitro* markedly decrease pathology and improve cognition *in vivo*. Neuron 2013; 80: 402–14.